Eigenray method: Caustic identification

Igor Ravve and Zvi Koren, Emerson*

Summary

At the last SEG meeting we presented the Eigenray method for finding stationary traveltime ray trajectories in 3D smooth heterogeneous anisotropic media, by applying a non-linear finite element scheme. We applied the Newton method that requires both gradient and Hessian of the traveltime with respect to nodal locations and ray velocity directions. In this study, we focus on the identification of caustic points and their types along the stationary path in order to account for the phase shift of the complex-valued Green's functions. The same finite-element scheme used for the stationary path is also used to analyze the second variation of the traveltime governed by the Jacobi differential equations, which leads to the same resolving matrix. The proposed method is unconditionally stable and more accurate than the commonly-used numerical integration methods of dynamic ray tracing equations, in particular for stationary rays passing through complex inhomogeneous anisotropic models with complex wave phenomena.

Introduction

Neighboring curved rays associated with the same seismic event can come together, or focus, to form an envelope or a caustic surface (e.g., Bott, 1982; Nye, 1985; Gutenberg and Mieghem, 2016; Červený, 2001, 2013). In these points along the ray, the cross-sectional area of the ray tube shrinks to zero, leading to anomalously large amplitudes (e.g., White et al., 1988). Since caustics affect Greens' functions involved in many physical problems, methods for their detection have been extensively studied. For 3D inhomogeneous general anisotropic media, Gajewski and Psencik (1987) suggested a finite-difference approach to establishing components of the transform matrix between the Cartesian and ray coordinates, and Garmany (2000) generalized the KMAH sign rule for caustics on convex and concave quasi-shear slowness surfaces. In the latter case, the curvatures of the slowness surface should be computed in order to draw conclusions about its convexity or concavity. Hanyga and Slawinski (2001) studied caustics and qSV rayfields of transversely isotropic and vertically inhomogeneous media. Waheed and Alkhalifah (2016) suggested an effective ellipsoidal model for tilted orthorhombic (TOR) media where the computed wavefield contains most of the critical components, including frequency dependency and caustics. Červený and Psencik (2017) applied a paraxial Gaussian beam approach to study wavefields at caustics and their vicinities, computing both geometric spreading and phase shifts in inhomogeneous anisotropic complex media. A comprehensive discussion on caustics is given in the book by Arnold (1994), with an extensive list of references therein. The conditions for the types of caustics can be derived from the Jacobian of the transform between the ray coordinates (RC) and ray-centered coordinates (RCC)**.** If only the determinant of the 2×2 Jacobian vanishes, we deal with a first-order caustic (line caustic). If both the determinant and the trace of the matrix vanish, this is a second-order caustic (point caustic). The cumulative number of phase shifts for complex-valued amplitudes along a ray represents the KMAH index named after Keller (1958), Maslov (1965), Arnold (1967) and Hörmander (1971). For isotropic media and for compressional waves in anisotropic media, a caustic increases the KMAH index by 1 or 2, depending on the caustic order. For shear waves in anisotropic media, the change in the KMAH index at a caustic can also accept negative values -1 and -2, since the slowness surface for these waves is not necessarily convex (Bakker, 1998; Červený, 2001; Klimes, 2010, 2014).

In this study we choose an alternative approach to caustics identification, applying the Jacobi second-order linear differential equation to detect caustics (Bliss, 1916). This equation governs the second traveltime variation due to infinitesimal changes in the ray path. The cited paper describes the Jacobi equation set for a multi-dimensional parametric functional. We adjust the functional for a stationary ray trajectory, where the characteristic parameter may be either the arc length *s*, the current time *t*, or parameter σ. Note that the traveltime between the endpoints, geometric spreading, locations and types (orders) of caustics and any other physical characteristics are independent of the choice of the characteristic parameter. The arc length *s*, however, seems the most suitable, due to a unit length of the path location derivative with respect to the arc length. We now apply the same finite element scheme which was previously used for the stationary path search to analyze the second variation of traveltime, described by the linear, second-order Jacobi ODE set. Unlike the boundary-value ray tracing problem, the Jacobi linear ODE set leads to a linear algebraic equation set after the finite element discretization. This means that no initial guess and no iterative procedure are needed. We apply the weak formulation and Galerkin method to the original second-order ODE set, thus effectively reducing it locally to a first-order weighted residual equation set. We use Hermite interpolation between the nodes, where the degrees of freedom (DoF) are the nodal values of the Cartesian components of the solution for the Jacobi equation set, and the derivatives of these components with respect to the arc length. The RC of the paraxial rays, γ_1 and γ_2, can be selected as initial value or boundary value conditions. The commonly-used initial

10.1190/segam2019-3216779.1

values are the direction angles' increments or plane wave locations' shifts at the source.

Jacobi Equation Set for Parametric Functional

The traveltime between the endpoints can be considered a parametric functional of the arc length s ,

$$t=\int_S^R L\left[\mathbf{x}(s),\mathbf{r}(s)\right]ds\ ,\quad \mathbf{r}=\frac{d\mathbf{x}}{ds}\ ,\quad \mathbf{r}\cdot\mathbf{r}=1\quad ,\qquad (1)$$

where $$L(\mathbf{x},\mathbf{r})=\frac{\sqrt{\mathbf{r}\cdot\mathbf{r}}}{v_{\text{ray}}\left[\mathbf{x}(s),\mathbf{r}(s)\right]}\quad .\qquad (2)$$

To conclude whether a stationary point is extreme or not, we need the second derivatives of the integrand with respect to both the location of the points along the ray path and the ray (group) velocity direction,

$$L_{\mathbf{xx}}=\frac{\partial^2 L}{\partial\mathbf{x}^2}=2\frac{\nabla_{\mathbf{x}}v_{\text{ray}}\otimes\nabla_{\mathbf{x}}v_{\text{ray}}}{v_{\text{ray}}^3}-\frac{\nabla_{\mathbf{x}}\nabla_{\mathbf{x}}v_{\text{ray}}}{v_{\text{ray}}^2}\quad ,\quad L_{\mathbf{rx}}=\frac{\partial^2 L}{\partial\mathbf{r}\partial\mathbf{x}}=\mathbf{L}_{\mathbf{xr}}^T\ ,$$

$$L_{\mathbf{xr}}=\frac{\partial^2 L}{\partial\mathbf{x}\partial\mathbf{r}}=-\frac{\nabla_{\mathbf{x}}v_{\text{ray}}\otimes\mathbf{r}}{v_{\text{ray}}^2}+2\frac{\nabla_{\mathbf{x}}v_{\text{ray}}\otimes\nabla_{\mathbf{r}}v_{\text{ray}}}{v_{\text{ray}}^3}-\frac{\nabla_{\mathbf{x}}\nabla_{\mathbf{r}}v_{\text{ray}}}{v_{\text{ray}}^2}\quad ,$$

$$L_{\mathbf{rr}}=\frac{\mathbf{I}-\mathbf{r}\otimes\mathbf{r}}{v_{\text{ray}}(\mathbf{x},\mathbf{r})}-\frac{\mathbf{r}\otimes\nabla_{\mathbf{r}}v_{\text{ray}}+\nabla_{\mathbf{r}}v_{\text{ray}}\otimes\mathbf{r}}{v_{\text{ray}}^2(\mathbf{x},\mathbf{r})}+2\frac{\nabla_{\mathbf{r}}v_{\text{ray}}\otimes\nabla_{\mathbf{r}}v_{\text{ray}}}{v_{\text{ray}}^3(\mathbf{x},\mathbf{r})}$$

$$-\frac{\nabla_{\mathbf{r}}\nabla_{\mathbf{r}}v_{\text{ray}}}{v_{\text{ray}}^2(\mathbf{x},\mathbf{r})}\ ,\qquad (3)$$

where subscript $\mathbf{x}$ is related to location, and $\mathbf{r}$ to direction. $L_{\mathbf{xx}}, L_{\mathbf{xr}}, L_{\mathbf{rx}}, L_{\mathbf{rr}}$ are square matrices of dimension 3. Vectors $\nabla_{\mathbf{x}}v_{\text{ray}}$ and $\nabla_{\mathbf{r}}v_{\text{ray}}$ are spatial and directional gradients of the ray velocity respectively. Tensors $\nabla_{\mathbf{x}}\nabla_{\mathbf{x}}v_{\text{ray}}$ and $\nabla_{\mathbf{r}}\nabla_{\mathbf{r}}v_{\text{ray}}$ are spatial and directional Hessians of the ray velocity; $\nabla_{\mathbf{x}}\nabla_{\mathbf{r}}v_{\text{ray}}$ and $\nabla_{\mathbf{r}}\nabla_{\mathbf{x}}v_{\text{ray}}$ are mixed Hessians. Ravve and Koren (2019) provide a computational workflow to establish these gradients and Hessians in smooth inhomogeneous anisotropic media.

There are two necessary conditions for a minimum (maximum): a) matrix $L_{\mathbf{rr}}$ should be positive-definite (negative-definite) at any point of the stationary path, and b) there should be no caustics along the path. The first condition is local, while the second is global. When both conditions are satisfied, they also become sufficient (e.g., Gelfand and Fomin, 2000). Zero is one of the eigenvalues for matrix $L_{\mathbf{rr}}$, and the corresponding eigenvector is the ray direction (Bliss, 1916). For isotropic media, the two other eigenvalues are $1/v$. The matrix becomes positive-semidefinite, but since the eigenvector is directed along the ray, we can treat it as positive-definite. Thus, for any isotropic media, the local condition for a minimum is always satisfied, and this makes a maximum traveltime path impossible. Obviously, this statement will hold for weak anisotropy. Although it has not been proven for media with strong anisotropy, one can assume that it is unlikely that traveltime maxima exist. Consequently, a caustic-free stationary path delivers a traveltime minimum, and that with one or more caustics is a saddle point.

The second condition for an extreme time path – the absence of caustics – is governed by the linear, second-order Jacobi equation set with variable (arc length dependent) coefficients (Bliss, 1916)

$$\frac{d}{ds}\left(L_{\mathbf{rx}}\cdot\mathbf{u}+L_{\mathbf{rr}}\cdot\dot{\mathbf{u}}\right)=L_{\mathbf{xx}}\cdot\mathbf{u}+L_{\mathbf{xr}}\cdot\dot{\mathbf{u}}\quad ,\qquad (4)$$

where $\mathbf{u}$ is the normal component of a paraxial ray and $\dot{\mathbf{u}}$ is its derivative with respect to the arc length of the central ray.

Solutions normal to the ray require an additional constraint,

$$\mathbf{u}\cdot\mathbf{r}=0\ \rightarrow\ d(\mathbf{u}\cdot\mathbf{r})/ds=\dot{\mathbf{u}}\cdot\mathbf{r}+\mathbf{u}\cdot\dot{\mathbf{r}}=0\quad .\qquad (5)$$

Since one of the three linear second-order equations is dependent (Bliss, 1916), the number of fundamental solutions reduces from 6 to 4 for 3D space (and from 4 to 2 for 2D). A second-order differential equation requires two initial or two boundary conditions. In this study, we consider paraxial rays emerging from a point source. Consequently, there are no ray path variations at this point, $\mathbf{u}_S=0$. The freedom remains for the second condition only, and thus, the number of independent fundamental solutions further reduces twice: two solutions for 3D and a single solution for 2D. For 2D, the signed distance between the solution and the ray path reads, $c=\mathbf{u}\times\mathbf{r}\cdot\hat{x}_2$, where x_1x_3 is the ray path plane, and $\hat{x}_2$ is a unit vector in the direction normal to this plane. Vanishing c is the caustic criterion. For a 3D case, there are two independent normal solutions, $\mathbf{u}_1$ and $\mathbf{u}_2$. While they do not necessarily intersect the ray path, their linear combination does in the case of a caustic. This means that the two solutions become collinear, and the following criterion, $c_L=\mathbf{u}_1\times\mathbf{u}_2\cdot\mathbf{r}$, vanishes. For 3D, caustics are distinguished by the order. The above mentioned vanishing criterion means a first-order (line) caustic. A second-order (point) caustic is defined by the vanishing criterion: $c_P=(\mathbf{u}_1\times\mathbf{r})^2+(\mathbf{u}_2\times\mathbf{r})^2$. Hence, in the case of a line caustic, a linear combination of the two fundamental normal Jacobi solutions vanishes. In the case of a point caustic, each normal solution vanishes separately.

The ray coordinates (RC), γ_1 and γ_2, may be chosen freely, for example, either the receiver location's shifts, or the ray direction's increments at the source.

Finite Element Formulation for Jacobi Set Solver

We derive the weak finite element formulation in order to solve the second-order Jacobi set. Weak formulation means that we relax the continuity of the solution to C_1. The

10.1190/segam2019-3216779.1

second derivatives need not exist and will not appear in the resulting set. The proposed finite element discretization is the same discretization used to obtain the Eigenray stationary ray path, with Hermite interpolation between the nodes. Thus, both the nodal function values and the nodal derivatives with respect to the arc length are independent DoF. We introduce the internal flow parameter within a finite element, ξ, $-1 \le \xi \le +1$. We multiply the Jacobi equation 4 by a weight (test) function w, integrate over the element length, and apply integration by parts. We obtain,

$$\int_{\xi=-1}^{\xi=+1} \left(L_{\mathbf{rx}} \cdot \mathbf{u} + L_{\mathbf{rr}} \cdot \dot{\mathbf{u}}\right) w' \, d\xi + \int_{\xi=-1}^{\xi=+1} \left(L_{\mathbf{xx}} \cdot \mathbf{u} + L_{\mathbf{xr}} \cdot \dot{\mathbf{u}}\right) w \, d\xi = \left(L_{\mathbf{rx}} \cdot \mathbf{u} + L_{\mathbf{rr}} \cdot \dot{\mathbf{u}}\right) w \Big|_{\xi=-1}^{\xi=+1} , \quad (6)$$

where dot means a derivative with respect to the arc length, while prime means a derivative with respect to the internal parameter ξ. We note that the weak formulation in equation 6 does not include the second derivative $\ddot{\mathbf{u}}$. The nodal values of the solution and its derivative are unknown, and Hermite interpolation is applied between the nodes. With the Galerkin method, widely used in the finite element approach, the test (weight) functions $w(\xi)$ are the same as the interpolation functions. Thus, there are $2n$ interpolation functions, where n is the number of nodes in a finite element. The left side of equation 6 leads to the local "stiffness" matrix (of a single finite element) which coincides with the local traveltime Hessian. Thus, the global stiffness represents the global traveltime Hessian as well, which was already computed on the last iteration of the stationary path search, $\mathbf{S}_{\text{glb}} \equiv \nabla\nabla t$. The right side of equation 6 yields the blocks of the local load vector. However, only the source S and receiver R nodes contribute to the right side, because at the joint nodes, the contribution of adjacent elements is cancelled,

$$\mathbf{f}_{\mathbf{x}}^{S} = -L_{\mathbf{rx}}^{S} \mathbf{u}_S - L_{\mathbf{rr}}^{S} \dot{\mathbf{u}}_S \quad , \quad \mathbf{f}_{\mathbf{x}}^{R} = +L_{\mathbf{rx}}^{R} \mathbf{u}_R + L_{\mathbf{rr}}^{R} \dot{\mathbf{u}}_R \quad , \quad (7)$$

Eventually, we solve the linear set,

$$\mathbf{S}_{\text{glb}} \hat{\mathbf{u}}_{\text{glb}} = \mathbf{f}_{\text{glb}} \quad , \quad (8)$$

where subscript "glb" means global (related to all nodes), and vector $\hat{\mathbf{u}}$ includes both $\mathbf{u}$ and $\dot{\mathbf{u}}$, subjected to the initial or boundary conditions. The additional constraints of equation 5 enforce the nodal solution vectors to be normal to the central ray.

Numerical Example: Diving Wave

Caustics may occur in layered media with discontinuous increase of the velocity gradient (e.g., Murphy, 1961; Bott, 1982; Nye, 1985; Cygan, 2006, and many others). The simplest representation of such a medium is a constant velocity layer over a constant velocity gradient half-space. We assume the following parameters: the layer thickness, $z = 3\text{km}$, its velocity, $v_a = 3\text{km/s}$, and the half-space gradient, $k_0 = 1\text{km/s}$. The velocity is continuous at the interface, but the gradient is not, and the second derivative of the velocity explodes. To apply the Eigenray approach, we smooth the velocity profile along the vertical axis. In a medium with this velocity model, a diving wave is possible only for offsets exceeding a definite threshold minimum, $h_{\min}$. For any offset exceeding the minimum value, two diving waves co-exist (multi-arrivals). The ray with a lower take-off angle is caustic-free, while that with a higher take-off angle exerts a caustic. For a minimum-offset ray, a single diving wave exists, with a caustic located exactly at the destination point.

The ray paths computed in the caustic-generating medium are shown in Figures 1a (the ray with the pre-critical take-off angle), 1c (post-critical angle) and 1e (critical angle). Eight three-node finite elements were used, and the corresponding segments of the paths are shown by different colors. For each case, the gray dashed line shows an initial guess. For the pre-critical ray, the initial path is an elliptic arc, given the offset, the take-off angle, and the maximum depth. For the post-critical ray, the initial path is a hyperbole, given the offset, the maximum depth and the radius of curvature at the apex. The computed traveltimes are very close to the analytical traveltimes, with minor discrepancies caused by smoothing of the gradient discontinuity needed for the numerical analysis.

Note that while the stationary path of the deep diving wave (caustic-free) and the trivial straight-line path, connecting the source and the receiver, are true traveltime minima, the stationary path of the shallow ray (with the caustic) represents a saddle point. The chance of obtaining the path of the true traveltime maximum is unlikely; such a maximum normally does not exist. However, a saddle point may be the case where a ray path has a minimum time (or a minimum Hamilton action in particle mechanics) with respect to some nearby alternative curves, and a maximum with respect to others (e.g., Gray and Taylor, 2007). We checked the eigenvalues of the traveltime Hessian matrix for the finite element scheme for the stationary ray, to make sure that this is indeed a saddle point. One of the eigenvalues proved to be negative, and the others are positive. To detect caustics, we applied the proposed Jacobi finite element solver for the three rays mentioned above, with offsets $h = 1.2 h_{\min}$ and $h = h_{\min}$. The caustic criterion, $c(s) = \mathbf{u} \times \mathbf{r} \cdot \hat{x}_2$, is plotted in Figures 1b, 1d and 1f vs. the arc length: for the caustic-free trajectory (deep ray path), for trajectory with the caustic and the same offset (shallow ray path), and for trajectory with the caustic at the receiver point (diving wave with the minimum offset). These caustics are of the first order (line caustics).

10.1190/segam2019-3216779.1

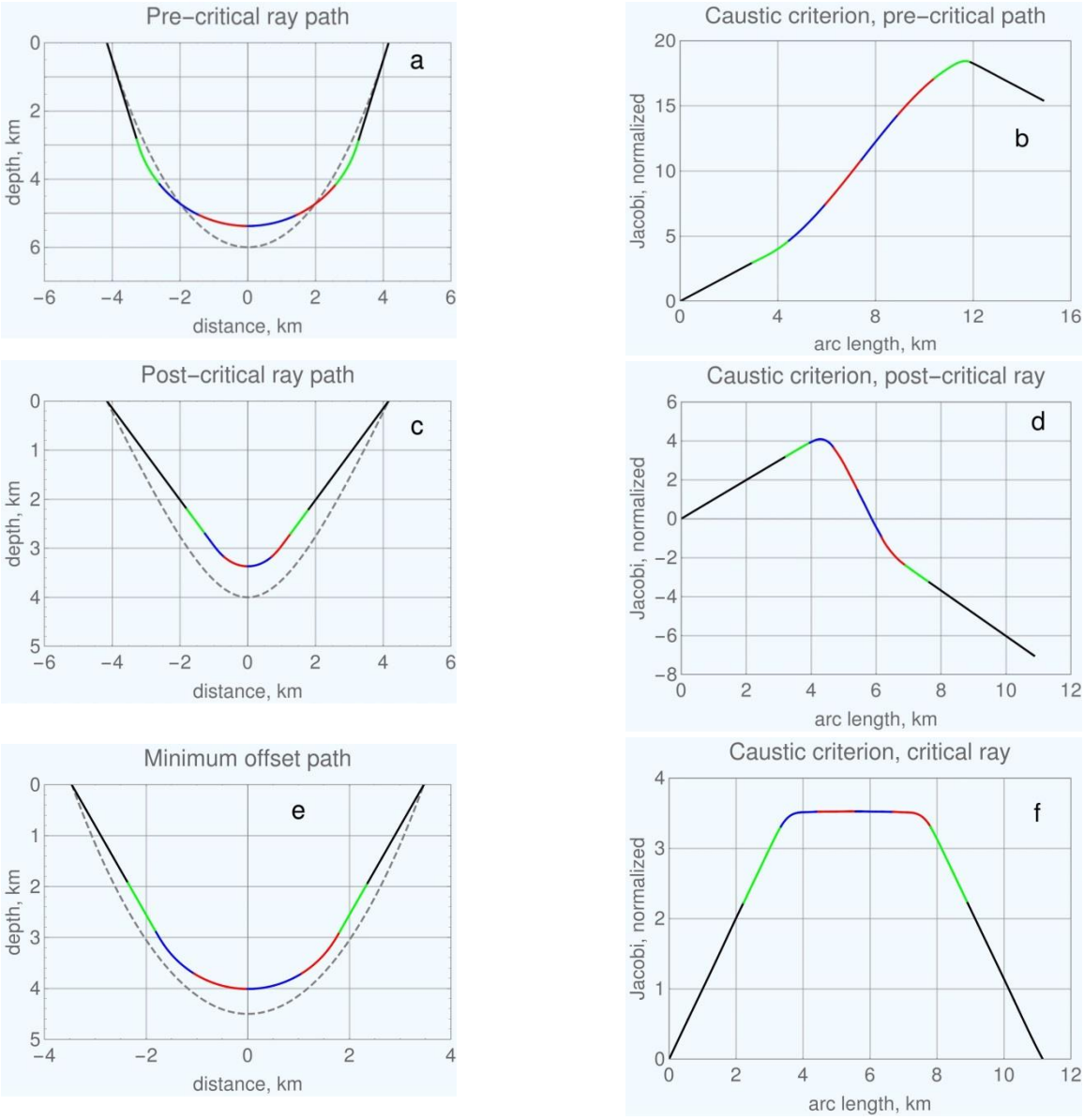

Figure 1: Central and paraxial ray paths in caustic-generating medium: a) Pre-critical ray path (deep, caustic-free), b) Caustic criterion for pre-critical ray path, c) Post-critical ray path (shallow, with caustic), d) Caustic criterion for post-critical ray path, e) Critical ray path with caustic at receiver point, f) Caustic criterion for critical path

Conclusions

We analyse the stationary ray path for caustics in 3D smooth heterogeneous general anisotropic media. Unlike the traditional approach for solving conventional dynamic ray tracing (DRT) equations, we suggest an alternative DRT set of equations obtained from the second traveltime variation for a stationary ray path, formulated as the Jacobi, second-order, linear ODE set. Instead of the traditional numerical integration approach, we apply the weak formulation and solve the resulting set with an accurate finite element implementation with Hermite interpolation. This is particularly important for the type of stationary rays studied in this work, involving caustics phenomena along waves traveling in complex geological areas.

10.1190/segam2019-3216779.1

REFERENCES

Arnol'd, V., 1967, Characteristic class entering in quantization conditions: Functional Analysis and Its Applications, **1**, 1–13, doi: https://doi.org/10.1007/BF01075861.

Arnold, V., 1994, Topological invariants of plane curves and caustics: American Mathematical Society.

Bakker, P., 1998, Phase shift at caustics along rays in anisotropic media: Geophysical Journal International, **134**, no. 2, 515–518, doi: https://doi.org/10.1046/j.1365-246x.1998.00574.x.

Bliss, G., 1916, Jacobi's condition for problems of the calculus of variations in parametric form: Transactions of the American Mathematical Society, **17**, 195–206.

Bott, M., 1982, The interior of the earth: Structure, contribution and processes: Arnold.

Červený, V., 2001, Seismic ray theory: Cambridge University Press.

Červený, V., 2013, A note on two-point paraxial travel times: Studia Geophysica et Geodaetica, **57**, no. 2, 267–275, doi: https://doi.org/10.1007/s11200-012-0373-6.

Červený, V., and I. Psencik, 2017, Elementary Green function as an integral superposition of Gaussian beams in inhomogeneous anisotropic layered structures in Cartesian coordinates: Geophysical Journal International, **210**, 561–569, doi: https://doi.org/10.1093/gji/ggx183.

Cygan, S., 2006, Modeling with seismic ray tracing in inhomogeneous geological formation: Geologia, **32**, no. 4, 451–462.

Gajewski, D., and I. Psencik, 1987, Computation of high-frequency seismic wavefields in 3-D laterally inhomogeneous anisotropic media: Geophysical Journal International, **91**, 383–411, doi: https://doi.org/10.1111/j.1365-246X.1987.tb05234.x.

Garmany, J., 2000, Phase shifts at caustics in anisotropic media, *in* L. Ikelle and A. Gangi, eds., Anisotropy 2000: Fractures, converted waves and case studies: Proceedings of the Ninth International Workshop on Seismic Anisotropy: SEG, 419–425.

Gelfand, M., and S. Fomin, 2000, Calculus of variations: Prentice Hall.

Gray, C. G., and E. F. Taylor, 2007, When action is not least: American Journal of Physics, **75**, no. 5, 434–458, doi: https://doi.org/10.1119/1.2710480.

Gutenberg, B., and J. Mieghem, 2016, Physics of the Earth's interior: Academic Press.

Hanyga, A., and M. A. Slawinski, 2001, Caustics in qSV rayfields of transversely isotropic and vertically inhomogeneous media, *in* L. Ikelle and A. Gangi, eds., Anisotropy 2000: Fractures, converted waves, and case studies: Proceedings of the Ninth International Workshop on Seismic Anisotropy: SEG, 409–418.

Hörmander, L., 1971, Fourier integral operators: Acta Mathematica, **127**, 79–183, doi: https://doi.org/10.1007/BF02392052.

Keller, J. B., 1958, Corrected bohr-sommerfeld quantum conditions for nonseparable systems: Annals of Physics, **4**, 180–188, doi: https://doi.org/10.1016/0003-4916(58)90032-0.

Klimes, L., 2010, Phase shift of the Green tensor due to caustics in anisotropic media: Studia Geophysica et Geodaetica, **54**, no. 2, 259–289, doi: https://doi.org/10.1007/s11200-010-0014-x.

Klimes, L., 2014, Phase shift of a general wavefield due to caustics in anisotropic media: Seismic Waves in Complex 3-D Structures, **24**, 95–109.

Maslov, V., 1965, Theory of perturbations and asymptotic methods (in Russian): Moscow State University Publication.

Murphy, D. A., 1961, Calculations of caustic lines in an ocean of constant velocity gradient layers: The Journal of the Acoustical Society of America, **33**, no. 6, 840–841, doi: https://doi.org/10.1121/1.1936835.

Nye, J. F., 1985, Caustics in seismology: Geophysical Journal International, **83**, no. 2, 477–485, doi: https://doi.org/10.1111/j.1365-246X.1985.tb06498.x.

Ravve, I., and Z. Koren, 2019, Directional derivatives of ray velocity in anisotropic elastic media: Geophysical Journal International, **216**, no. 2, 859–895, doi: https://doi.org/10.1093/gji/ggy445.

Waheed, U.B., and T. Alkhalifah, 2016, Effective ellipsoidal models for wavefield extrapolation in tilted orthorhombic media: Studia Geophysica et Geodaetica, **60**, no. 3, 349–369, doi: https://doi.org/10.1007/s11200-015-1151-z.

White, B., B. Nair, and A. Bayliss, 1988, Random rays and seismic amplitude anomalies: Geophysics, **53**, no. 7, 903–907, doi: https://doi.org/10.1190/1.1442527.